Design and Fabrication of Ultrasound Phantoms to Identify the Actuator of Arterial Wall Longitudinal Movement

Sandra Sjöstrand & Alice Widerström

2015

LUND
UNIVERSITY

Master's Thesis in Biomedical Engineering

Faculty of Engineering LTH
Department of Biomedical Engineering

Supervisor: Magnus Cinthio
Assistant Supervisor: Hans W. Persson

Abstract

Although a decade has passed since the longitudinal movement of arteries was shown *in vivo*, the cause for this multiphasic movement has not yet been established. Pressure as a force driving the forward motion has been repeatedly dismissed on the grounds that pressure acts perpendicular to the wall and therefore solely in the radial direction. In this work we have shown in a simplified theoretical model and phantom models that pressure can cause a longitudinal movement of vessel phantoms of some specific geometries. The compound phantoms were produced using a combination of traditional and innovatory techniques. The phantoms were in two parts and PVA was used for both. A system to connect the phantom inlet to a pump was also developed. The phantoms where designed such that any movement due to pressure could be isolated.

The result showed that the geometry and position influenced the longitudinal movement. A comparison of the magnitude of the movements of three different phantoms showed that the movement was smallest in the phantom where pressure could not generate a large forward movement according to the theory. The geometry of this particular phantom was a cylinder of constant diameter, and the lengthening was measured to 0.186 mm with a standard deviation of 0.057. The other geometries involved a decrease of the diameter, one gradual and another abrupt. The lengthening was 3.258 ± 0.077 and 5.375 ± 0.392 mm respectively.

The movement pattern along the length of one of the phantoms strongly indicate that the largest part of the movement originates where pressure would have the greatest influence.

This implies that the pressure can drive the forward motion of the vessel wall.

Sammanfattning

Trots att ett decennium har gått sedan artärernas longitudinella rörelse visades *in vivo* är bakgrunden till denna multifasiska rörelse fortfarande inte fastställd. Att trycket skulle kunna driva rörelsen har ledigt avfärdats. Resonemanget har varit att eftersom trycket verkar vinkelrätt mot väggen kan det endast påverka den radiella töjningen. I följande arbete har vi visat i en förenklad teoretisk modell samt i fantom-modeller att trycket kan orsaka en longitudinell rörelse hos kärlfantomer med vissa specifika geometrier. En kombination av traditionella och nyskapande tekniker användes för att skapa de sammansatta fantomerna. Fantomerna gjordes i två delar och PVA användes till båda. Ett system för att koppla samman fantomen med en pump utvecklades. Fantomerna designades så att en eventuell tryckdriven rörelse kunde isoleras.

Resultatet visade att geometrin påverkade storleken av den longitudinella rörelsen. En jämförelse av rörelsens omfattning mellan tre olika fantomer visade att rörelsen var minst för den fantom där trycket inte skulle kunna orsaka en stor framåtrörelse enligt teorin. Geometrin för denna fantom var en cylinder med konstant diameter och förlängningen uppmättes till 0.186 mm med en standardavvikelse på 0.057. De andra geometrierna hade en minskande diameter, den ena gradvis, den andra abrupt. Förlängningen var 3.258 ± 0.077 respektive 5.375 ± 0.392 mm.

Rörelsemönstret längst med en av fantomerna är också en stark indikation på att större delen av rörelsen härrör från den position där trycket skulle ha störst påverkan. Detta tyder på att trycket verkligen kan driva en framåtriktad rörelse av kärlväggen.

Preface

This project was carried out during the spring term 2015 at LTH, Lund Unversity. It was a continuation of previous research done by Åsa R. Ahlgren and Magnus Cinthio. The aim of the project was to build ultrasound phantoms to be used for investigation of the longitudinal movement of arteries.

We would like to thank Matilda Larsson of Stockholm Univestity for an inspirational meeting prior to the project start. Thank you for sharing your knowledge on compound phantom design.

From the department of Chemical Engineering we would like to thank Ola Wallberg for lending us a working pump. For your effort and enthusiasm in understanding our requirements and searching the far corners of LTH to find it.

From the department of Biomedical Engineering we would like to thank Axel Tojo, who showed us how to operate the 3D printer and related software. Special thanks for the patience shown regarding technical problems.

Désirée Jarebrant for assisting with all the administrative work and for lending us your key every time with a smile.

Maria Evertsson, for kindly showing us how to make Agar and PVA. Your previous experience with the materials and your written and verbal instructions facilitated the work greatly.

Roger Andersson, John Albinsson and all the other people who thought about, talked about and worked with the pump system.

Hans W. Persson, our assistant supervisor, for help and suggestions regarding this thesis.

Magnus Cinthio, our supervisor, for believing in us and giving us this opportunity. For being committed and giving up so much of your time to progress this project. For your eternal optimism.

Contents

1 Introduction

1.1 Background

The cardiovascular system is complex, and the properties of the blood vessels are central to understanding hemodynamic processes fully (Nichols et al., 2005). Cardiovascular diseases is today the most common cause of death globally. In 2008, an estimated 17 million people died from cardiovascular disease (Mendis et al., 2011). If the risk for cardiovascular diseases can be detected early, the quality of the patients life can be improved but also money could be saved on reduced health care costs (Purwanto et al., 2012). Preventive measures against, and treatment of, cardiovascular disease have indeed reduced cardiovascular mortality in high income countries during the last decades of the 20'th century (Mendis et al., 2011). Currently, risk factors such as hypertension, diabetes and dyslipidaemia are used as indicators (Mendis et al., 2011).

During the cardiac cycle, the common carotid artery experiences a radial expansion and contraction as well as a distinct multiphasic longitudinal movement (Cinthio et al., 2006). Figure 1 illustrates the perpendicular directions.

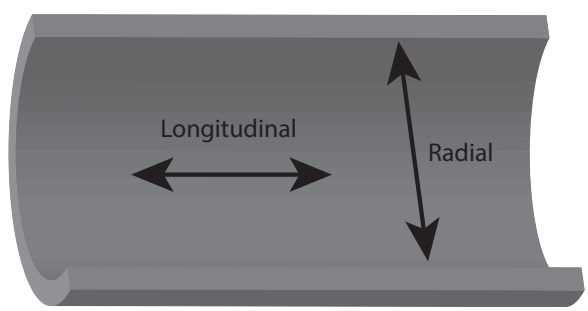

Figure 1: Illustration of radial and longitudinal movement

The radial movement of the arteries has been known for a long time, and is today measured to determine the arteries stiffness, for example by using ultrasound (Laurent et al., 2006). Moreover, increased arterial stiffness is an independent risk factor for cardiovascular mortality (Laurent et al., 2001). Little attention has previously been given to the longitudinal movement of the arteries, as it was thought to be negligibly small compared to the radial movement. Furthermore, the longitudinal

movement was assumed to be due to the movement of the diaphragm from breathing (Nichols et al., 2005). In the early 21st century it was discovered that this movement was larger then previously though, in fact it was in the same magnitude as the radial (Cinthio et al., 2005). Current research indicate that the longitudinal movement is driven by pressure (Ahlgren et al., 2012a) and not by shear stress (Ahlgren et al., 2015). These results are still unconfirmed in humans.

Recent studies have found a specific connection between reduced longitudinal movement of the common carotid artery and risk factors for cardiovascular disease (Zahnd et al., 2012). This, we consider, motivates further investigation of the cause and implications of the phenomenon.

1.2 Aim

This study aims to isolate the actuator(s) of longitudinal movement of arteries. The study will be conducted by designing and manufacturing suitable phantoms, to be used in ultrasound measurements. Thus, the aim can be separated into several parts.

1. Designing and manufacturing phantoms for investigation of longitudinal movement in arteries. Key points include
   (a) design and fabricate a phantom consisting of two parts; one vessel and a support structure mimicking surrounding tissue
   (b) designing a system to transfer liquid from a pump into the phantom
   (c) designing a system to transfer liquid out of the phantom
   (d) ensuring that longitudinal movement of the phantom wall is possible
   (e) creating molds for casting the phantoms
2. Investigate with ultrasound, using the phantoms, the role of pressure as a factor driving longitudinal movement of arteries.
   (a) measure the longitudinal displacement
   (b) compare three different geometries

A deeper understanding of the hemodynamic processes could conduce to new methods of early diagnosis, and a greater understanding, of cardiovascular disease.

2 Theory

2.1 Arteries

Arteries, the blood vessels transporting blood from the heart out to the body, consist of several layers; intima, media and adventitia. The innermost, and thinnest layer is the intima, followed by the muscular and usually thickest layer called media. Adventitia is the outermost layer, consisting largely of connective tissue, see figure 2. Between the media and the adventitia is a thin layer, made of elastic connective tissue, called the external elastic lamina (Kwon et al., 1999). The aorta is 10-20 mm in diameter and it narrows distally. The thickness of the intima and media combined is less than 1 mm and it increases with age. For a healthy 20 year old, the thickness is around 0.5 mm and at 70 years old the thickness has increased to around 0.9 mm (Lindgärde et al., 2009).

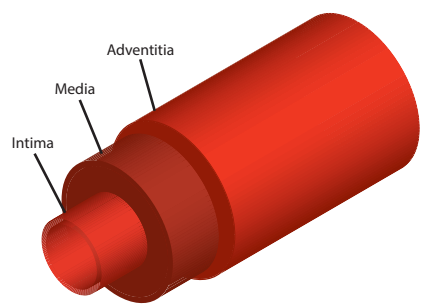

Figure 2: The layered structure of an artery. The external elastic lamina, located between media and adventitia, is not shown in the image.

Arterial wall stiffness refers to the ability of major vessels to expand and contract radially in pace with the pressure. The vessels get stiffer if there is an increased formation of collagen and a decreased amount of elastin. Atherosclerosis can also affect the stiffness (Lindgärde et al., 2009). Arterial wall stiffness has been shown to be an independent risk factor for cardiovascular mortality (Laurent et al., 2001).

2.2 Longitudinal movement

The longitudinal movement of the common carotid artery is distinctly multiphasic, bidirectional and cyclic, coinciding with the pulse. The common carotid artery is a proximal artery. Proximal arteries are elastic (Nichols et al., 2005) and exhibit a large longitudinal movement. Distal arteries are more muscular and less elastic but longitudinal movement is present in distal arteries as well (Cinthio et al., 2006). In early systole there is a movement forward, in the direction of the blood flow. Later in systole this is followed by a retrograde movement. In diastole a second forward movement occurs and then the wall gradually returns to it's original position (Cinthio et al., 2006). The pattern of the longitudinal movement of the common carotid artery is different between different persons (Ahlgren et al., 2012b). Measurements performed on 10 healthy humans shows that the average first forward longitudinal movement of the common carotid artery is 0.39 mm. The inter subject deviation is large. But the greatest movement does not exceed 1 mm (Cinthio et al., 2006). The first forward movement will be compared to results for the phantoms.

The movement is largest by the vessel lumen but present at the adventitia as well. Although the movement is smaller at the adventitia it still exhibits each of the phases (Cinthio et al., 2006).

2.3 Forces along the arterial wall

There are several forces acting along the vessel wall that could potentially influence the longitudinal movement. These include shear stress from blood, pressure, pulse wave and pulse wave reflection (Ahlgren et al., 2012a). The properties of the blood, mainly that it belongs to the non-Newtonian, shear thinning liquids, also influence the flow profile (Gijsen et al., 1999) and forces originating from the blood. In addition certain physiological processes, such as breathing, left ventricle contraction and activity of the smooth muscles, might affect or cause the longitudinal movement (Ahlgren et al., 2012a). Wall shear stress caused by the blood flow acts on the inner surfaces of the vessels along the direction of flow. It is dependent on the blood velocity gradient at the vessel wall (wall shear rate) and of the blood viscosity. The wall shear rate increases with increased blood velocity. New studies show no correlation between the longitudinal displacement and the wall shear rate and thus, the wall shear stress (Ahlgren et al., 2015).

The same study shows, together with a previous publication, (Ahlgren et al., 2012a), a positive correlation between pulse pressure and longitudinal displacement of the arterial wall.

Pressure acts perpendicular to a surface (Young et al., 2004), and in a simplified model of a blood vessel, such as a hollow cylinder, pressure would have no component along it. This model is however insufficient; the aorta bends and bifurcates into smaller vessels. In figure 3 four examples of different vessel geometries are shown. In addition the lumen undergoes continuous radial contraction and dilation during the cardiac cycle (Nichols et al., 2005). This creates areas were pressure can act and potentially cause longitudinal movement of the artery.

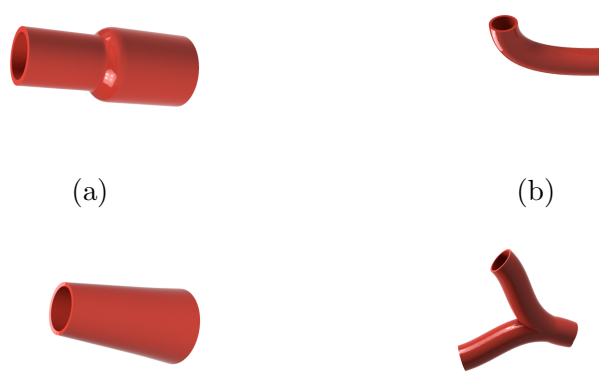

(a) (b)

(c) (d)

Figure 3: Vessel geometries where pressure could act in the direction of flow: (a) Abrupt diameter change, (b) Curved vessel, (c) Decreasing diameter, (d) Bifurcation. Direction of flow is from right to left in the images.

Pulse waves are generated due to the pulsatile nature of the flow. The blood pressure varies in pace with the heart beat. The maximal pressure, the systolic pressure, occurs after the ventricular contraction. The lowest blood pressure, called the diastolic pressure, occurs when the heart relaxes. In a young healthy human the pressure varies between 80-120 $mmHg$ (Nationalencyklopedin, 2015b). Recent experiments have shown that adrenaline (commonly produced during mental stress (Nationalencyklopedin, 2015a)) can increase the longitudinal movement of

the aortic arteries (Ahlgren et al., 2009). Moreover administration of drugs affecting blood pressure showed that the magnitude of the longitudinal movement increased with pressure (Ahlgren et al., 2012a). This could be an indicator that pressure drives the longitudinal motion.

Reflections of the pulse waves occur due to variations of the vascular impedance. These can be due to branching, change of diameter or change in stiffness. The effects of such reflections are many and have been extensively studied. Increased wave reflection in proximal arteries has been observed in patients with increased arterial stiffness (Nichols et al., 2005). Pulse wave reflection as a driving force for longitudinal movement has not yet been thoroughly investigated and cannot be ruled out (Cinthio et al., 2006). In the common carotid artery the longitudinal movement pattern seems to be related to the arrival of the pulse wave, the reflected pulse wave and the rereflected pulse wave from the heart (Cinthio et al., 2006).

When flow dynamics are modeled for larger vessels it is not necessary to take the non-Newtonian properties of blood into account (Zamir, 2000).

Breathing will cause movement artefacts but when patients were asked to hold their breath during the examination, distinct longitudinal movements were still present (Cinthio et al., 2005).

Left ventricle contraction causes the top part of the heart to displace (Ahlgren et al., 2012a). If this was driving the motion one would expect proximal arteries to move but not distal. However longitudinal movement seems to be present in all large arteries, including popliteal, abdominal and brachial (Cinthio et al., 2006).

Contraction, reorientation and relaxation of the smooth muscle of the media could contribute to the measured longitudinal movement. Reorientation of the smooth muscles seems to occur when the length of the artery alters. It is however not clear if the smooth muscle play an active role in driving the longitudinal movement, or if it is a byproduct of it (Ahlgren et al., 2012a).

2.4 Theoretical mathematical model

In this section an expression relating pressure to longitudinal movement is developed. Figure 4 shows the model phantom that will be used.
A pump is rigidly fixed to the inlet of the phantom, to the left in figure 4. When it is started it instantaneously generates a high pressure, p_{in}. As a

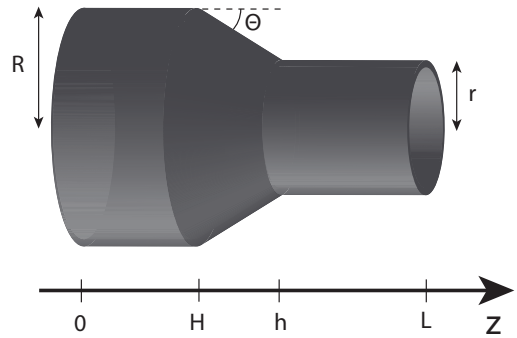

Figure 4: Model phantom of length L. From $0 < z < H$ the outer radius is constant and equal to R, the radius then narrows with an angle of Θ and from h to L it is equal to r. The wall thickness t is much smaller than r.

simplification, we will assume that pressure drops at the phantom inlet and then remains constant throughout the phantom until the outlet, where the pressure is p_{out}. This can be described by equation 1. Here the pressure $\mathbf{p}$ is a vector in space and $\hat{n}$ is the unit vector normal to the inclined surface

$$\mathbf{p}(z) \cdot \hat{n} = p = \begin{cases} p_{in} & z \leq 0 \\ p_{in} - \Delta p & 0 < z < L \\ p_{out} & z \geq L \end{cases} \tag{1}$$

In equation 1, L denotes the full length of the phantom and Δp is the pressure drop at the inlet.

The pressure causes a plain stress state where the radius is constant. Hooks law, for planar stress, using polar coordinates, states that

$$\begin{cases} \varepsilon_r = -\frac{\nu}{E}[\sigma_\phi + \sigma_z] \\ \varepsilon_\phi = \frac{1}{E}[\sigma_\phi - \nu\sigma_z] \\ \varepsilon_z = \frac{1}{E}[\sigma_z - \nu\sigma_\phi] \end{cases} \tag{2}$$

where ε is the strain, σ is stress, E is Young's modulus and ν is Poisson's ratio. Expressions for the stresses are found by balancing equations assuming thin walled cylinders

$$\begin{cases} \sigma_z \pi 2r(z)t = p\pi r(z)^2 \implies \sigma_z \approx \frac{pr(z)}{2t} \\ \sigma_\phi 2Lt = p2(r(z)-t)L \implies \sigma_\phi \approx \frac{pr(z)}{t} \\ \sigma_r \approx p \ll \sigma_z, \sigma_\phi \end{cases} \tag{3}$$

Three cases will be discussed; First a cylinder of constant radius r, second a shape like in figure 4 but with $\Theta = 90°$ and finally a case with $\Theta = 45°$. For a straight cylinder of length L and constant radius r, the length alteration can be calculated as

$$\delta_z = \int_0^L \varepsilon_z dz = \frac{Lp}{E}\Big(\frac{r(1-2\nu)}{2t} + \nu\Big) \tag{4}$$

For the case where $\Theta = 90°$, the pressure causes a force on the circular disk at the radius change. This force depends on the surface area of the disk and is equal to

$$F = p\pi(R^2 - r^2) \tag{5}$$

F acts on the cylindrical tube, the cross sectional area of which is A. The expression for the length alteration due to the force on the disk, δ_d, is given by

$$\delta_d = \frac{FH}{AE} = \frac{p(R^2 - r^2)H}{2RtE} \tag{6}$$

The total length alteration for this geometry is a sum of three parts, one due to the force on the disk and one for each of the cylindrical sections of radius R and r. These are denoted with the subscripts d, R and r and respectively. $\delta_{tot} = \delta_d + \delta_R + \delta_r$, see equation 7

$$\begin{aligned} \delta_{tot} &= \frac{p(R^2 - r^2)H}{2RtE} \\ + \frac{Hp}{E}\Big(\frac{R(1-2\nu)}{2t} + \nu\Big) &+ \frac{(L-h)p}{E}\Big(\frac{r(1-2\nu)}{2t} + \nu\Big) \end{aligned} \tag{7}$$

In this expression any deformation of the disk has not been taken into account. The final case involves a cone shaped transition between the wide and narrow cylinders. The deformation of the cylinders can be deduced using the same method as above, any deformation of the cone will be disregarded. The length alteration due to the pressure on the cone, δ_c, depends on the surface area and the angle Θ. The surface area

is lager for the cone than for the disk. Given the angle Θ and the radii R and r, the area is equal to

$$A_c = \frac{\pi(R^2 - r^2)}{\sin\Theta} \tag{8}$$

The same pressure, p acts on this surface but only the sine component acts in the longitudinal direction. The force in the z-direction is thus

$$F_c = p\sin\Theta A_c = p\pi(R^2 - r^2) \tag{9}$$

and the total length alteration is again given by equation 7. There are a few things to be said based on this model. Firstly that pressure can give rise to a length alteration in a rotationally symmetrical geometry. There can be several components to the strain. Since the pressure acts radially it produces a strain component in the z-direction according to equation 2. Additionally, the pressure acts on any incline surface along the geometry, producing a forward force depending on the surface area and angle of incline. When this force is calculated for a constant pressure it is noted that only the difference in radius is important. Thus one would expect the longitudinal movement to be greater for a geometry with decreasing radius than for one with constant radius. No consideration has been taken to a possible deformation of the disk and cone. Further the pressure is constant in these calculations, this is also a simplification since the pressure probably varies in the phantom, especially where the radius changes.

2.5 Ultrasound

An ultrasound image is produced by transmitting a sound pulse and recording the echo. Echos are produced where there is a difference in acoustic impedance between two regions. The acoustic impedance is the resistance of a medium when subjected to a pressure. A B-mode (brightness mode) image is a two dimensional slice of the object under investigation. The plane represented by the image is called the image plane. Each pixel is assigned a shade between black and white. The lighter the shade, the stronger the echo. The vertical position is decided by the time it took for the echo to return and the set speed of sound, assumed to be constant (Hoskins et al., 2010). In an ultrasound image the two innermost layers of the artery, intima and media, cannot be

resolved from each other. They are therefore often referred to as one, called the intima-media complex (Lindgärde et al., 2009).

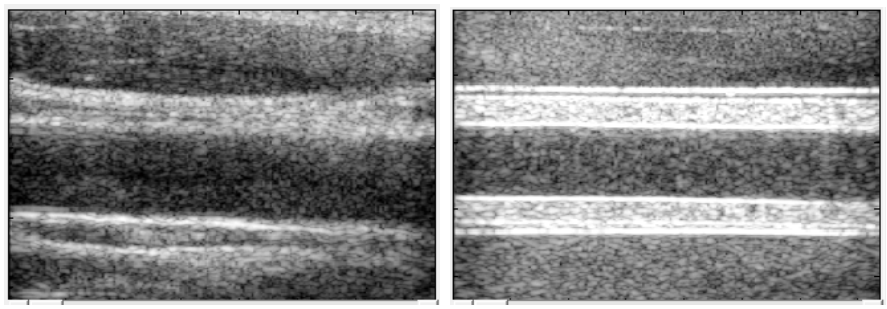

(a) (b)

Figure 5: Ultrasound image of (a) human common carotid artery and (b) one of the phantoms designed and fabricated. The images are not produced with the same magnification.

Speckle-tracking is a method to measure movement in an ultrasound image. A specific echo, chosen by the user, is followed in consecutive time frames. Speckle-tracking works well while the movement occurs within the image plane. If the transducer is carelessly angled the supposedly tracked echo might move in and out of the image plane resulting in false readings (Cinthio et al., 2005).

3 Method

3.1 Setup

The materials and equipment used to carry out the measurements of the phantom movements will be described in detail below. First an overview of the setup is presented. The whole setup can be seen in figure 6. A schematic view is shown in figure 7.

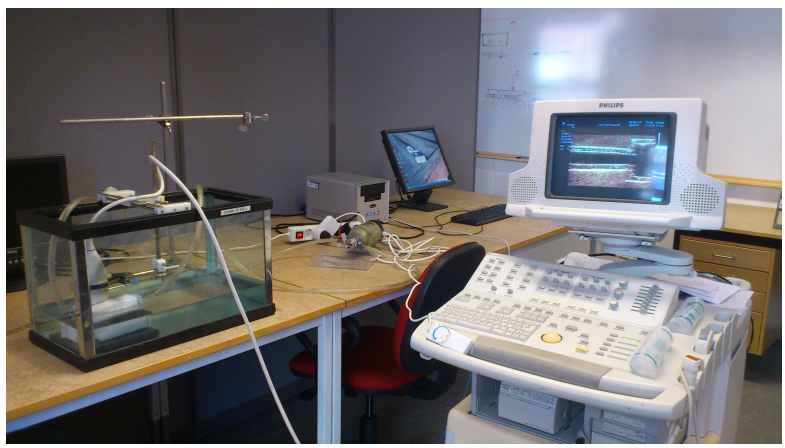

Figure 6: Experimental setup

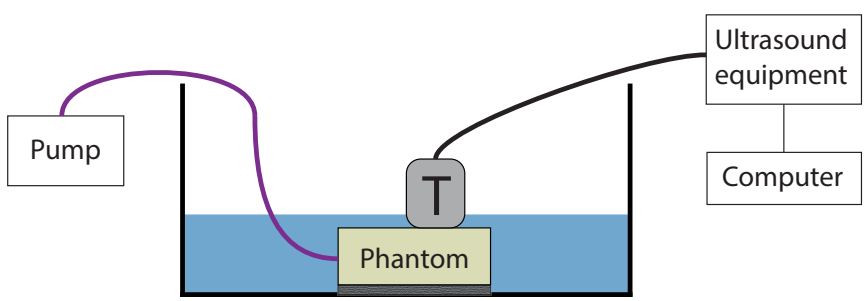

Figure 7: Schematic view of of the experimental setup

The pump was connected to the phantom via flexible tubes. Water was used to mimic blood. Two rubber bands were used to secure all the parts of the phantom together. The compound phantom was then placed in a water filled tank on a rubber slab. The water reached to

the top of the supporting structure. The slab prevented strong echos from the bottom of the tank and kept the phantom from sliding. The ultrasound transducer was kept in position by a clamp attached to a holder on the top of the tank. When movement was recorded as a function of distance from the inlet, the transducer was positioned at three different positions along the phantom. For all other measurements the transducer was placed close to the outlet of the phantom.

3.2 Pump

To pump the water a Magnet Gear Pump from Iwaki Co., Ltd. Kanda Suda-cho, Chiyoda-ku, Tokyo, was used. Flexible tubes were connected to the pump and filled with water before the pump could be started. The pump was controlled using a dimmer. The pump seemed to reach maximum capacity after the dial on the dimmer was turned approximately 90°. This point was marked and all measurements were carried out by alternating between the off position and this marking.

3.3 Phantom

The phantoms needed to be manufactured in a way to make it possible for the ultrasound equipment and speckle-tracking algorithm to detect the presence of a longitudinal movement. The phantoms were manufactured in two parts. The first one representing the intima-media complex and a second part mimicking the adventitia and the surrounding tissue. The two phantom parts needed to be able to glide against each other to make the movement possible. The physiological analogy is the external elastic lamina. In the arteries the longitudinal movement is larger for intima-media complex than for adventitia, and so a sliding movement seems to take place at the external elastic lamina.

3.4 Molds

In the CAD program Fusion 360, Autodesk, San Rafael, CA, USA, 3D models of each part for the molds were designed. The models were converted into instructions for 3D printing using the software Cura, Ultimaker B.V., Geldermalsen, Netherlands. Finally the parts were made from PLA (Polylactic acid) using the 3D printer Ultimaker 2, Ultimaker B.V., Geldermalsen, Netherlands. The printer builds the molds layer by layer, applying melted PLA from a nozzle. The plastic hardens quickly

making it possible to add the next layer almost immediately. Where convenient, parts were cut out using a milling machine or milk cartons were used. The cartons were square with two sides of 70 mm and were cut to a height of 150 mm.

3.5 Phantom materials

3.5.1 Agar

Agar is a gelatinous substance obtained from algae (Encyclopedia Britannica, 2015). In order to evaluate agar as a phantom material a simple test was carried out. Three different concentrations of agar (1%, 0.7% and 0.5%) were mixed and prepared by centrifugation, heating until boiling point and then an additional cycle of centrifugation. The agar was poured into plastics cups and left to cool and solidify. Pieces of 3D-printed PLA were added into two of the cups to determine if the plastic would retain its shape and if the two materials could be separated later.

3.5.2 PVA

Another option for making the phantoms was the water-soluble polymer PVA (Polyvinyl alcohol) in crystal form (Sigma-Aldrich, 2015). Ten percent PVA crystals was mixed into milli-Q water. The mixture was heated to 98 $°C$ until the PVA crystals were completely dissolved, approximately 3 hours. The mixture was stirred every half hour. When completely dissolved, the PVA was left to cool. This was done for two types of PVA with different molecular weights, 31-50 kg/mol and 85-124 kg/mol. The solution was frozen for 12 hours and thawed at room temperature for an additional 12 hours. The freeze thaw cycle was carried out twice. A test was preformed where a piece of PLA was added to PVA to determine if the phantom could be easily separated from the PLA mold. The finished PVA casts needed to be kept in water, to avoid desiccation.

3.5.3 Glass beads

The movement tracking algorithm requires a strong and distinct echo. This is provided by glass beads with mean diameter of 93 μm (Potters Industries, Valley Forge, PA, USA). 5 $g/liter$ was added to the chosen phantom material.

3.6 Ultrasound equipment and measurements

To obtain the ultrasound images of the phantom a HDI 5000 SonoCT from Philips Medical Systems, Bothell, WA, USA was used. The transducer used was a L12-5 from ATL, Inc., Bothell, WA, USA, with a 38 mm broad field of view. During a measurement a couple of seconds long image sequence, showing the movement, was recorded. The acquired images were sent to a computer were the software HDI-lab transformed the data to a suitable file format, to be used with the software Matlab, MathWorks, Natick, MA, USA, which was used for tracking the movement.

3.7 Speckle-tracking

A speckle-tracking algorithm was used to determine the movement of the vessel phantom wall (Albinsson et al., 2014). The ultrasound machines HD-zoom was used in the vertical direction to magnify the relevant area. In the first picture from the ultrasound sequences obtained, a region of interest (ROI), 11×7 pixels, approximately 0.55×0.35 mm, was positioned to contain a distinct echo from a bead. The movement of this echo was then tracked. The position of the ROI was chosen at the far wall when possible. This was the position that would work best with the program executing the algorithm. If there was no strong echo or to much disturbance from air bubbles in the water, an echo from the wall nearest to the transducer was chosen. When the deformation was recorded as a function of distance from the inlet, consistency was very important. Therefore, all ROI:s were placed on the near transducer wall where disturbance due to bubbles within the lumen cannot occur. The distance from the phantom inlet was found in the following manner; First the distance from the inlet to the center of the transducer was measured using a ruler. The width of the field of view was specified as 38 mm. With this information the horizontal position in the phantom corresponding to each ROI placement in the image could be determined.

3.8 Pressure and flow sensors

Two transducers from Keller AG, Winterthur, Switzerland, were used to measure the pressure and flow. A interface converter, K-114 from Keller, was used to connect the sensors with the computer. Keller also provided the software, CCS30, that collects and displays the data. The

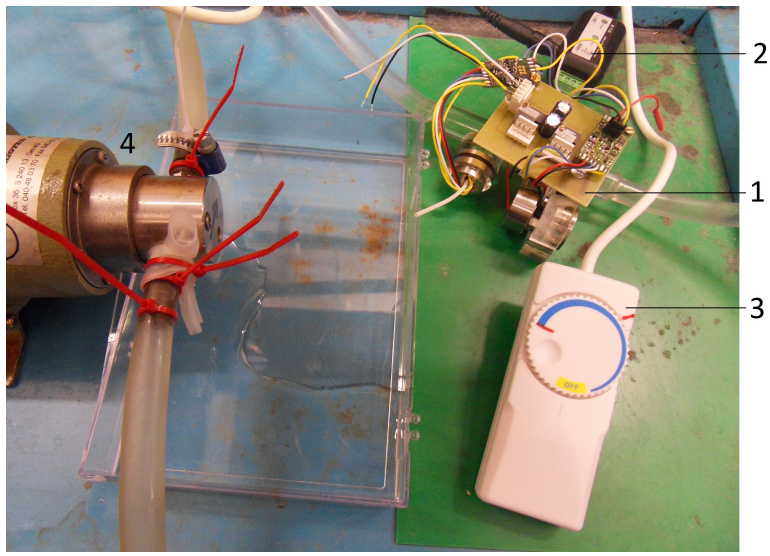

Figure 8: Setup for pressure and flow measurement. The pressure and flow sensor is seen in the top right corner, indicated by the number 1. The interface converter, 2, is connected to the sensors. The dimmer, 3, used to control the pump is below the sensor. Part of the pump is visible to the left, 4.

transducers were mounted into a plastic holder. The sensors are inserted into a open ended cylinder through which a liquid can pass. A vegetable based oil was used to link the pressure inside of the tube to the sensor. The measurement was carried out by pumping water through the tubes used too connect the phantom to the pump. The cylinder with the sensors was connected instead of the phantom. The setup can be seen in figure 8. The pressure and flow were measured simultaneously while alternating the output of the pump between zero and the red marking.

4 Results

4.1 Developed equipment

4.1.1 Molds

Three sets of ultrasound phantoms were made. Since the phantoms were in two parts, for each phantom there were two separate molds. To cast the vessel phantom, a mold in six parts was used, see figure 9.

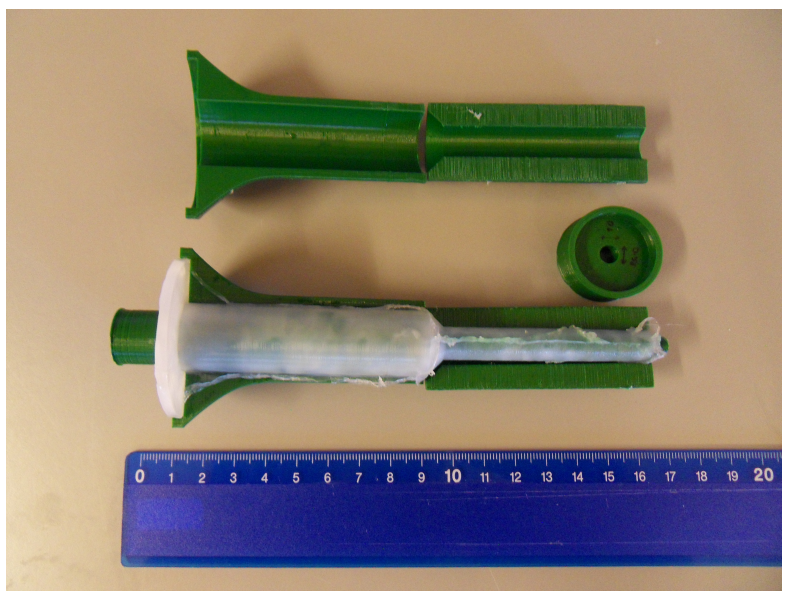

Figure 9: Mold for vessel phantom consisting of six parts. At the top of the image two parts creating the outside contour can be seen. The circular disk to the right forms the base of the mold. Below in the image is a finished phantom with the rod shaping the inner contour still in place. The ruler is graded in *cm*.

There are two main reasons for using so many parts for this mold. Primarily to make it easier to extract the phantom when cured. Secondly that the same parts could be used to cast another vessel geometry, where this was possible.

The vessel phantom needed a brim for the connection to the pump. Due to the bottom-up technique of the 3D printer, the outer diameter of the molds needed to increase gradually, see figure 9. The mold was assembled and secured using electrical tape. The tape also prevented the PVA from leaking out of the mold.

The supporting structure was cast in a four part mold, see figure 10. PVA was poured into a carton. The hole was created by centering a 3D

Figure 10: Mold for support structure, in front the rods creating the hole for the three different geometries. In the back the carton with lid and frame (the latter two are white in the image).

printed rod using a square plate. The rod was held in place by a lid and kept down with tape. The lid, along with a frame secured around the center of the carton, also prevents the carton from bulging.

4.1.2 Selecting materials

PVA with the molecular weight 85-124 kg/mol with added glass beads was selected for the final phantom prototype. PVA was selected due to its superior properties regarding durability. Agar, when handled, was easily torn while PVA retained its shape. Further more, PVA released readily from the PLA mold. The PVA crystals with greater molecular weight was chosen since fewer freeze and thaw cycles was needed for the PVA to cure, two cycles were sufficient. The glass beads produce distinct echos, suitable for tracking with the algorithm. For the supporting structure we excluded glass beads since no motion would be tracked here.

4.1.3 Phantom design

The phantom was constructed in two parts. One inner part mimicking the intima and media, and a second, outer part mimicking the surrounding tissue and adventitia. Figure 11 shows the compound phantom and the connection. Figure 12 shows a schematic drawing.

Figure 11: The compound phantom with inlet connection to the right in the image.

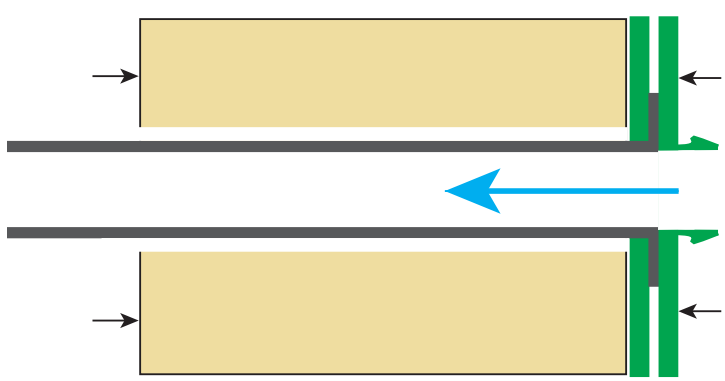

Figure 12: Section of the compound phantom; vessel phantom (gray), supporting structure (beige), inlet connection plates (green). The direction of flow is indicated by the blue arrow

The vessel phantoms were most critical; they were thin and sensitive to strain. Bubbles could get trapped and make a hole through the wall. The vessel phantom was designed in three different versions. One with an abrupt change in inner diameter ($\Theta = 90°$ in figure 3), from 16 mm to 6 mm, at half the phantom length, one intermediate with a gradual change in diameter ($\Theta = 45°$ in figure 3) and one control, with no diameter change see figure 13. The vessel phantoms were all designed with the same length of 140 mm.

The outer diameter of the vessel phantoms are approximately the same size as the human aorta which is slightly larger than the common carotid artery. The thickness of the wall is also greater than that of the common carotid artery. This decision to scale up the system was taken in consideration to durability and manageability. The brims were used to connect the phantom with the tube from the pump, see next paragraph.

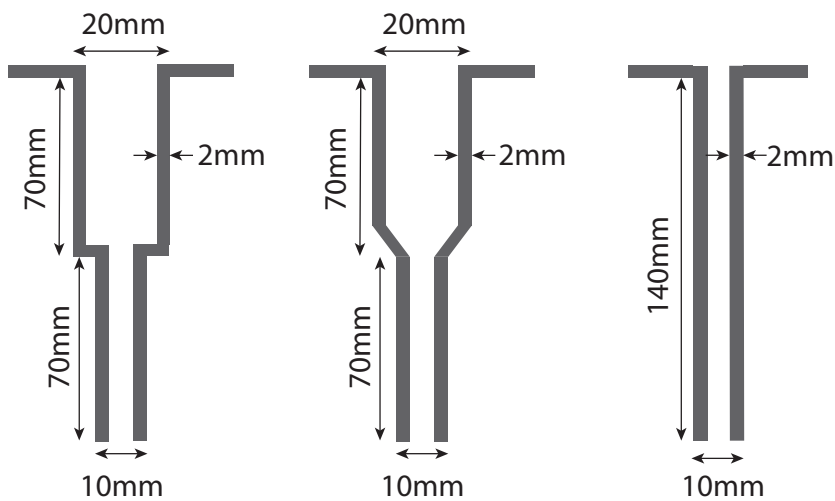

(a) (b) (c)

Figure 13: The different designs of the vessel part of the phantom. Figure (a) with an angel of 90° at the diameter change, figure (b) with an angel of 45° and figure (c) with no diameter change.

The supporting structures were manufactured to enclose the vessel. These consist of a rectangular block with a hole matching one of the vessel phantoms. To allow movement there is a margin of 1 mm between the outside of the vessel and the inside of the supporting structure. At

the diameter change for figure 13a and 13b a greater margin of around 4 mm was left, to allow as big movement as possible, see figure 14.

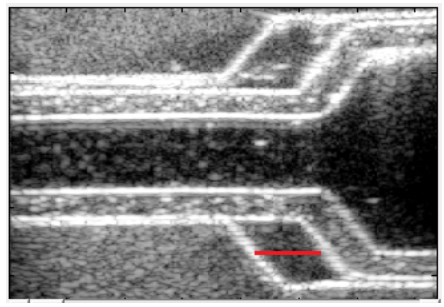

Figure 14: The vessel is placed with a 4 mm margin in the longitudinal direction from the supporting structure. The margin is marked with a red line.

When the ultrasound measurements were performed the transducer was placed directly on the supporting structure, close to the outlet. To get a good connection here the supporting structure should be flat. This is achieved by the square shape of the carton, retained by the frame during casting.

4.1.4 Inlet and outlet

The phantom was connected to the pump via an elastic tube. The connection was made by using two plates, one on either side of the vessel phantom's brim. The first plate was square with a circular hole through which the vessel fits. The second plate was similar but made with a funnel to which the hose could be attached, see figure 15. A section of the phantom can be seen in figure 12, the inlet plates are marked in green. The outlet was left free to allow maximum mobility.

4.2 Quantitative results

The pressure and flow measured from the magnet gear pump, used to drive the longitudinal movement, is shown in figure 16. The phantom was not connected when these results were obtained.

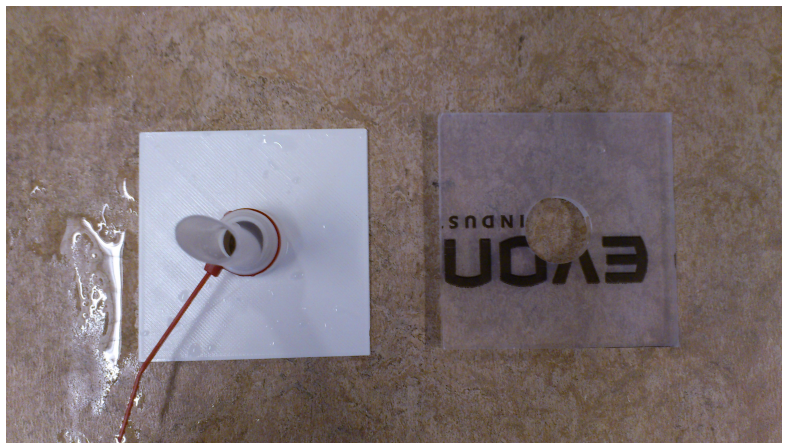

Figure 15: The two plates of the inlet. To the right the plate were the vessel fits. To the left the plate with the funnel where a hose is attached.

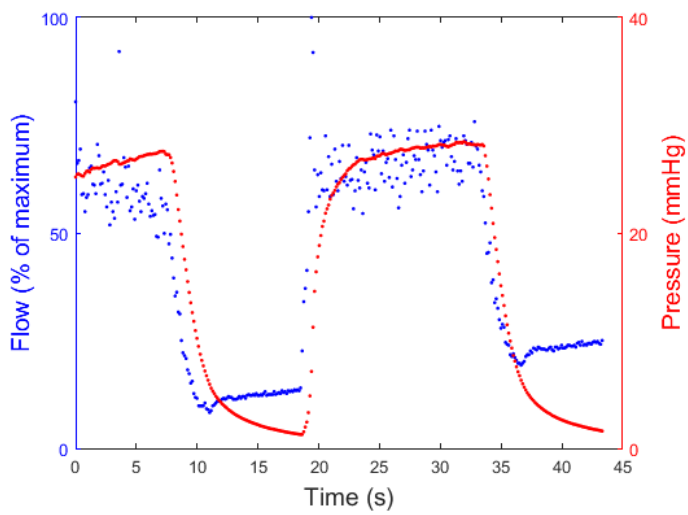

Figure 16: Flow and pressure curve obtained simultaneously, flow sensor not calibrated and drifting.

The longitudinal displacement of the phantoms was calculated using the speckle-tracking algorithm. Five measurements were carried out for each geometry. The transducer was placed close to the phantom outlet. The result for the straight, 0° phantom is shown in figure 17, the 45° phantom in figure 18 and the 90° phantom in figure 19. Notice that the scale is different between the figures.

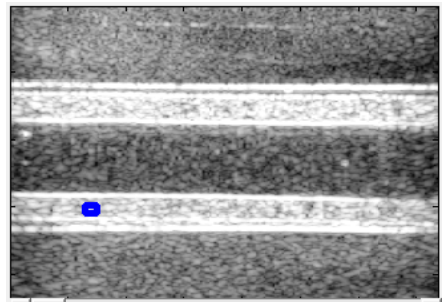

(a)

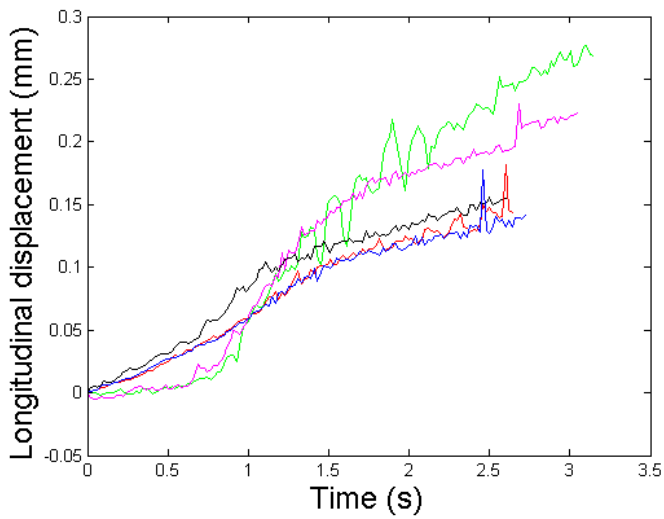

(b)

Figure 17: 0° phantom, the flow enters from the right. (a) The ultrasound image of the phantom, the blue rectangle is the region of interest tracked (b) The longitudinal displacement of the vessel phantom calculated with the echo-tracking algorithm.

The maximum displacement for the 0° phantom was 0.269 mm. The average displacement was 0.186 mm with the standard deviation 0.057.

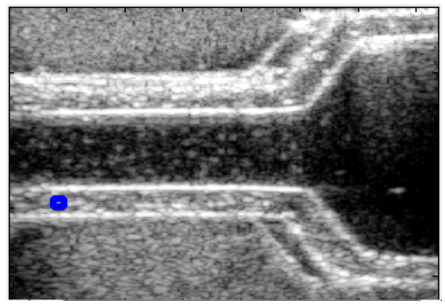

(a)

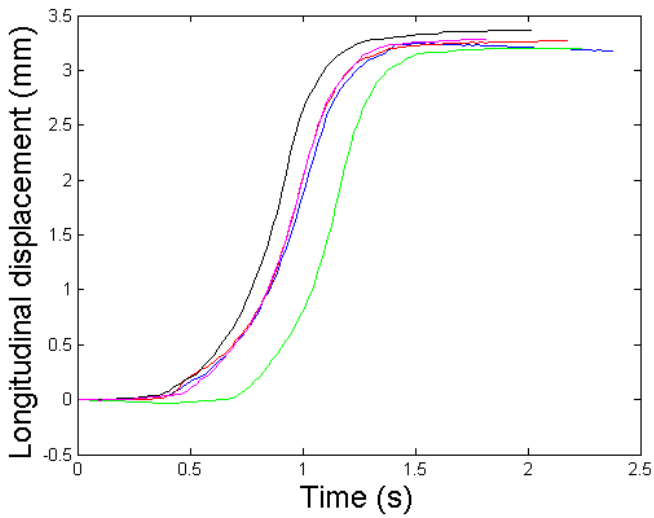

(b)

Figure 18: 45° phantom, the flow enters from the right. (a) The ultrasound image of the phantom, the blue rectangle is the region of interest tracked (b) The longitudinal displacement of the vessel phantom calculated with the echo-tracking algorithm.

The maximum displacement for the 45° phantom was 3.370 mm. The average displacement was 3.258 mm with the standard deviation 0.077.

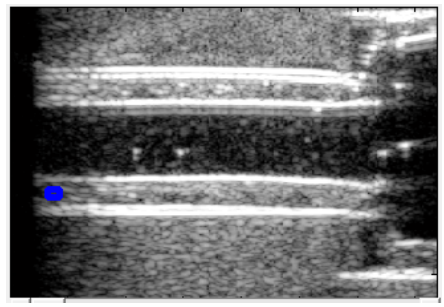

(a)

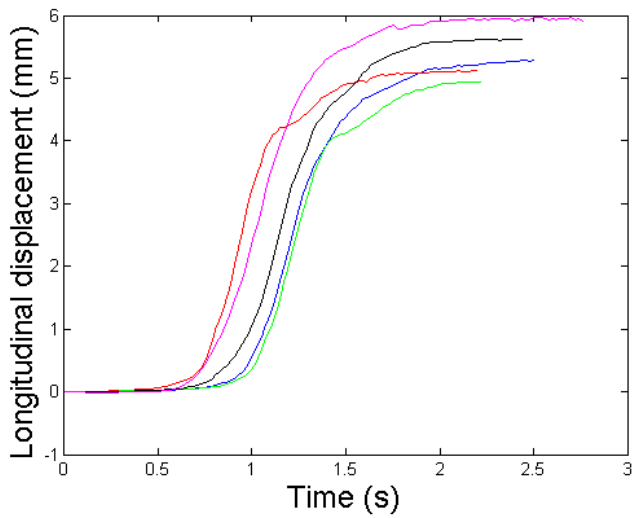

(b)

Figure 19: 90° phantom the flow enters from the right. (a) The ultrasound image of the phantom, the blue rectangle is the region of interest tracked (b) The longitudinal displacement of the vessel phantom calculated with the echo-tracking algorithm.

The maximum displacement for the 90° phantom was 5.916 mm. The average displacement was 5.375 mm with the standard deviation 0.392.

The longitudinal displacement measured close to the phantom outlet, plotted against the angle of the phantom, Θ in figure 4, is shown in figure 20.

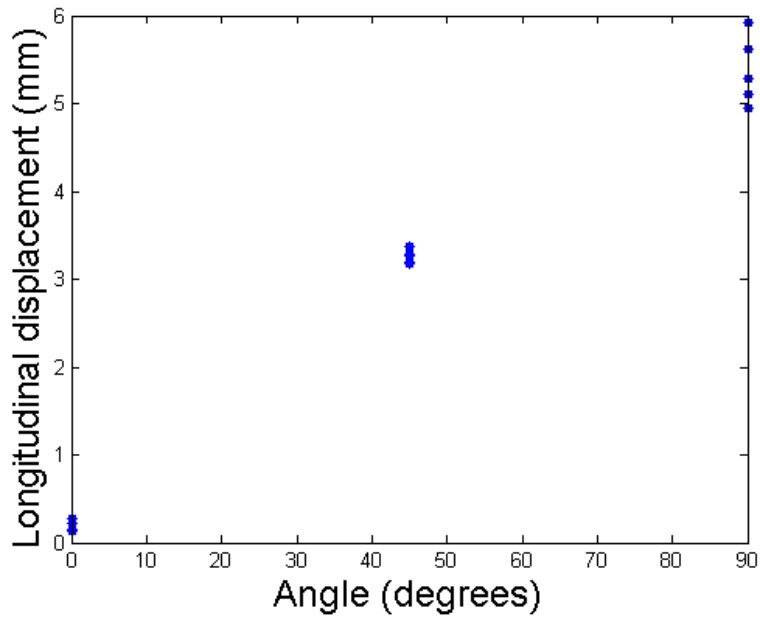

Figure 20: The longitudinal displacement plotted against the angle of the phantom. Five measurements were made for each angle. Each displacement was measured close to the outlet of the phantom.

In figure 21 the longitudinal displacement of the 45° phantom is plotted against the distance from the inlet. The displacement increase with the distance. The position of the beginning of the narrowing is marked with a red line.

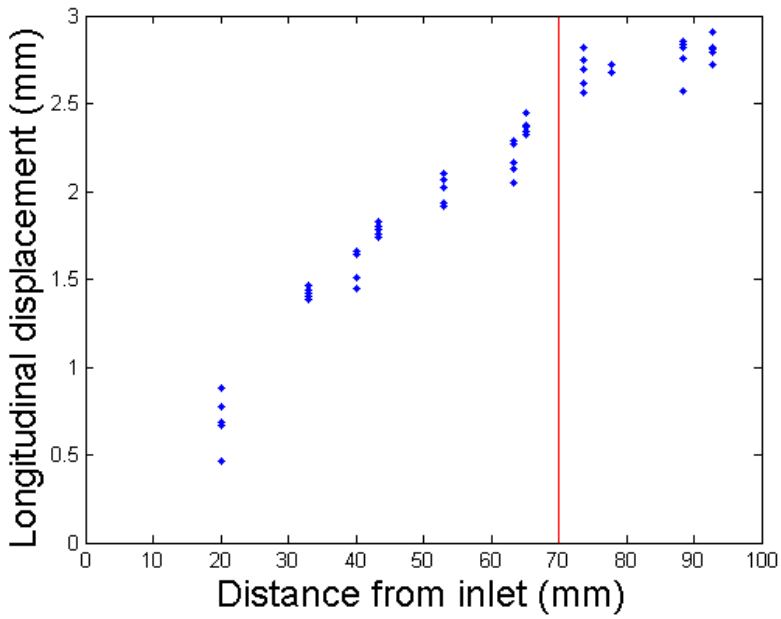

Figure 21: The longitudinal displacement plotted against the distance from the inlet. Measured on the 45° phantom. The red line marks the beginning of the narrowing.

5 Discussion

The aims defined in the first section of the report involve design and fabrication of phantoms and investigating these phantoms using ultrasound. The main focus of this project has been to design, manufacture and assemble the phantoms, item 1 of the aim. The finished phantoms consist of two PVA parts: one part that is moving, called the vessel phantom and a second, stationary part, called the supporting structure. The vessel mimicking phantom is cylindrical with a diameter and wall thickness of the same order of magnitude as the common carotid artery. The vessel phantom was designed with a brim in order to transfer liquid into it. Figure 15 shows the rest of the components used for the inlet. A system to control the transfer of liquid out of the phantom was developed but not fully implemented. The molds have been prepared so that a funnel can be secured at the outlet of the supporting structure. For this project however, it was sufficient that the outlet was left unobstructed. Longitudinal movement of the phantom wall was enabled by casting the phantom in two parts separated by a narrow spacing. Leaving the outlet free also facilitated the longitudinal movement. Three sets of phantom molds were produced, see figures 9 and 10. The molds needed to be in multiple parts so that the finished phantom could be easily extracted without breaking.

The second part of the aim involved conducting ultrasound measurements of the movement on three different geometries. The results from these can be seen in figures 17 to 19 and figure 21. Thus, each of the aims have been successfully met. The methods used will now be discussed focusing on limitations, implications and improvements. Finally the results are commented upon.

The shape and size of the phantoms were partly determined by the properties of the 3D-printer. The printer was used to make the molds. The dimensions chosen in Fusion 360 were not exactly what the printer produced. Generally, each printed line widened a few percent, sometimes in an asymmetrical manner. This made it difficult to fit parts together. We tried to compensate for this in our Fusion 360 designs. The printer builds the object from the bottom-up and the nozzle has a set width, so when designing this also need to be taken in to account.

When the vessel phantoms were fabricated air bubbles sometimes got caught, leaving a hole. These phantoms could not be used. The problem occurred repeatedly for the phantom with the abrupt diameter

change, figure 13a, before a faultless version was achieved. In an attempt to avoid this problem, the PVA solution was degassed using a vacuum pump. The pump produced a partial vacuum over several hours, forcing small bubbles to expand and rise to the surface. The attempt was unsuccessful for two reasons. The high viscosity of the 10%, high molecular weight PVA solution means that this method of degassing takes a very long time. During this time the glass beads would accumulate at the bottom of the flask. More importantly, when the PVA was poured into the mold pockets of air were formed producing new bubbles. Ultimately what worked was pouring the PVA very carefully and waiting for up to half an hour before placing it in the freezer. This would give any slow rising bubbles time to reach the surface before the material started to freeze.

After a couple of weeks the fabricated vessel phantoms changed their shape, they shrank. So ideally the measurements should be conducted soon after the fabrication of the phantoms. Since we had difficulties with the pump and other equipment and to save material and time, this was not always the case in this project. In one case we used to small quantities of PVA to cast the brim of a vessel phantom. The brim then became very thin and dried out quickly and the whole vessel phantom had to be discarded.

In our setup the vessel phantom was fixed in the inlet and at the outlet the phantom was left free. This is of course not the case in the human body. In the body the media is connected to the adventitia by the external elastic lamina. It is here the longitudinal movement is believed to take place. There are several reasons why the phantom turned out so different from the situation *in vivo* in this regard. One is that we needed to connect the pump in a way to avoid leakage. This forces the inlet to be rigidly fixed. Another reason was that is was very difficult to fabricate a phantom with a structure similar to the external elastic lamina. We considered fixing the outlet as well to make a more realistic setup. After consideration we decided not to do so, primarily since we wanted as big movement as possible. In continued research we believe it to be a good idea to make phantoms with a fixed outlet. This will make it possible to measure flow and pressure both before and after the phantom. It would be interesting to learn how the movement would be affected.

The phantoms were designed with space between the vessel and the supporting structure to give as big longitudinal movement as possible,

figure 14. In future phantom designs this gap could be removed, to give a more realistic movement.

The vessel phantoms are cylindrical, one with constant diameter as a reference, and two cases where the diameter changes. The vessel phantoms designed do not correspond to any existing artery in the body. The geometries are chosen to give us extreme cases, were the movement is either as big or as small as possible. This is one reason for the extent of the observed longitudinal movement.

It would be interesting to investigate the other cases in figure 3, such as a curved or bifurcating geometry, but this study is limited to the case of narrowing lumen, see figure 3a. It would also be interesting to study a more realistic narrowing lumen, were the diameter change is smaller and occurs gradually, as in the body.

We only manufactured phantoms for three different angles, 90°, 45° and 0°, see figure 13. It would be interesting to add results for phantoms with other angels, to better establish the dependence of the angle of the narrowing. This was not done in this project due to lack of time, and technical problems of the 3D-printer.

Initially, the project was focused around a pump and control unit able to generate flow profiles mimicking blood flow. Sadly this setup did not work. Initially, the problem was thought to be in the control unit, and so this was replaced. When the system did not work nonetheless a great deal of trouble shooting was carried out. This included finding and using manuals, for the motor and amplifier, soldering new contacts and parts for testing, measuring electrical signals and disassembling the motor to check the Hall sensors by hand. The problem was first thought to be due the amplifier and a new was ordered. It was not sufficient to solve the problem and a new motor had to be ordered as well. At the time for the submission of this thesis the system was almost operational but it was never possible for us to use it in any of our measurements.

To test our phantoms we instead used a simpler pump, varying the flow and pressure using a dimmer. We figured that this would suffice since we had an external pressure and flow sensor. The pressure from the pump was quite low, only around 25 $mmHg$, see figure 16. Using this pump we could not produce the type of flow profile like the pump we originally hoped to use. So in continuation of this project hopefully the more advanced pump system can be used.

In the experiments, water was used in place of blood, despite the fact that the two liquids have different properties. Water has a low

viscosity that is constant with stress whereas blood is a viscous, non-Newtonian liquid. Blood belongs to a group of non-Newtonian liquids that are shear thinning i.e the viscosity decreases with stress. These differences possibly influenced the outcome of the tests. Since the effects are smaller in larger vessels, we presume the influence to be small. To increase viscosity it is possible to mix glucose with the water.

The flow and pressure sensors used were sensitive to air. The ripple at the top in figure 16 is probably due to small air bubbles in the flowing water. The maximum pressure and flow measured would in this case increase if a bubble free flow could be established.

When using the Matlab script analyzing the movement, the position that the region of interest cursor was placed influenced the results. It was important that the vessel was placed horizontally in the ultrasound sequence to make sure the longitudinal movement was registered in the right magnitude. It was quite hard to establish, since the supporting structure's sides were not completely flat and both the ultrasound equipment and the supporting structure had a tendency to move. The vessel part was also not always situated horizontally in the supporting structure.

The Matlab script could also be used to determine the radial expansion. We tried to use it for our measurements, but sadly it did not work. Maybe since bubbles were present in the water, leaving strong echoes disturbing the tracking of the walls.

The result of the longitudinal movement are larger than in the human common carotid artery, the first forward longitudinal movement is on average less than half a millimeter. In our results the movement is a couple of millimeters. The phantoms were designed to maximize the possibility for longitudinal movement due to pressure. The diameter change is greatly exaggerated. The dimensions of the vessel phantoms, that is the external diameter and the wall thickness, are also slightly larger than *in vivo*. This is believed to act mainly as a hindrance to the movement since it increases the cross sectional area normal to the direction of flow.

The numerical results obtained are largely in agreement with what was expected. Pressure acting in the radial direction would give rise to a small lengthening of each of the phantoms. This was also observed since the endpoint of the straight phantom moved on average 0.186 mm. The phantom is fixed at the inlet and, according to the mathematical model, there is a parallel force due to pressure where the narrowing occurs. As

a result, the wide part of the phantom, between the inlet and the narrowing, experience a strain. The narrow part on the other hand mainly experience a parallel displacement. The parallel displacement is what was observed in the ultrasound images. This additional strain would not be present in the constant radius phantom and therefore the longitudinal displacement can be expected to be much larger for the phantoms with a decreasing diameter. This also happened and the average displacement for the 45° and 90° were 3.258 and 5.375 mm respectively. This is more than 10 times larger than for the 0° phantom. This implies that indeed pressure, and not shear stress, drives this movement. The difference in displacement for the 90° phantom compared to the 45° is not explained by the mathematical model. The model is very simplified and does not take into account a varying pressure or any deformation of the vessel.

The deformation of the cone shaped center is rather complicated. To find its deformation, one would have to model the system using the finite element method since the radius is dependent on the position in the z-direction. This was not covered in this work but would be interesting to investigate further. It would be interesting to model the other geometries also. In the ultrasound images it was clear that the narrowing parts both displaced and deformed when the pressure increased. The displacement is explained by the simple mathematical model, but not the deformation.

For the 45° we also measured the displacement along the whole vessel. The graph of movement as a function of distance, see figure 21, shows that the movement was smallest close to the inlet an largest further away. Moreover, the increase seems to be linear up until the narrowing of the phantom. After this the rate of change decreases. This is another clear indication that the diameter decrease is a critical point for the longitudinal movement. If the shear stress was a determining factor for the longitudinal displacement the pattern of movement would look different. In that case, the movement should increase where the phantom has the smallest diameter. The flow would be larger here and therefore the shear rate. Since the results show that the movement occurs in the wider part rather than the narrow, shear stress can be assumed to be negligible compared to pressure. These results are also in agreement with a recent study, (Ahlgren et al., 2015).

The geometries of the phantoms are such that a movement due to pressure can be isolated from a movement due to other forces. Factors

that affect the system *in vivo*, such as breathing, reorientation of smooth muscle cells and movement of the heart, are not present in the current set up. Moreover any movement due to shear stress would be larger in the narrow phantom, where pressure would cause the smallest movement according to the theory. Pulse waves and pulse wave reflections are also unlikely to influence the results since the pump does not work cyclically.

The results obtained here show that the pressure cannot be ruled out as a driving force for the longitudinal movement of vessels. Mainly, however, this work has been a proof of concept, and an initiation of another research project. In this work we have developed a method that can be used to investigate the pressure as a driving force for the longitudinal movement. We have also shown that pressure can be used to drive a forwards movement of a vessel. In our continued research, we aim to fabricate more phantoms, so that the relation between movement and angle can be thoroughly investigated and with sufficient data to preform statistical analysis.

6 Conclusions

To summarize, this work has shown how phantoms, that can be used to investigate the relation between pressure and longitudinal movement, can be produced; and that it is possible for pressure to induce a movement like the one that has been observed in arteries.

The phantoms were made out of the polymer PVA, in two parts. The first part is mimicking the blood vessel and the second the surrounding tissue. A small amount of glass beads was added to the PVA for the vessel phantom in order to ensure strong echos that could be used to track the movement. The vessel part was placed inside the second part. To cast the phantoms, plastic molds manufactured using a 3D-printer were used. The phantoms were designed and fabricated in three versions, all with different geometries. One of the phantoms had the same diameter through the whole length. For the two others the diameter changed at the middle: one abruptly and one more gradually, see figure 13.

The result presented in figure 20, shows that the phantom where the diameter remained constant moved little in the longitudinal direction. The phantoms with changing diameter moved much more, and the vessel phantom with an abrupt diameter change had the greatest displacement. So, the presence of a diameter change will enhance the longitudinal movement, and the angle of this diameter change will influence the magnitude of the movement.

Figure 21 shows the the movement is smallest at the inlet, where the phantom is attached, and increases with distance. Moreover that after the narrowing of the lumen, the rate of change of movement as a function of distance decreases or possibly subsides. This further reinforces the hypothesis that movement occurs due to the diameter change.

In the setup used, many of the possible actuators of longitudinal movement can be readily ruled out since they are simply not present. Others can be deemed unlikely after some reasoning and with support from the theory section. The pressure is still a likely actuator of the longitudinal movement of these phantoms.

Since these results were produced by using phantoms, it is difficult to comment upon what, if any, implications they have *in vivo*. A few things can however be said on the matter. Firstly that, since the arteries do become more narrow distally, a situation somewhat similar to the narrowing phantom does occur in the body. Secondly that the

diameter change that precede the longitudinal movement can also cause such a narrowing. Thirdly that the role of pressure in the longitudinal movement *in vivo* needs to be further investigated.

References

Ahlgren, Å. R., Cinthio, M., Nilsson, T., Persson, H. W., Lindström, K., Steen, S., and Sjöberg, T. (2012a). "Longitudinal displacement and intramural shear strain of the porcine carotid artery undergo profound changes in response to catecholamines." In: *American Journal of Physiology - Heart and Circulatory Physiology* 302.5, pp. 1102–1115.

Ahlgren, Å. R., Cinthio, M., Persson, H. W., and Lindström, K. (2012b). "Different Patterns of Longitudinal Displacement of the Common Carotid Artery Wall in Healthy Humans Are Stable Over a Four-Month Period." In: *Ultrasound in Medicine and Biology* 38.6, pp. 916–925.

Ahlgren, Å. R., Cinthio, M., Persson, H. W., Lindström, K., Steen, S., and Sjöberg, T. (2009). "Effects of adrenaline on longitudinal arterial wall movements and resulting intramural shear strain: A first report." In: *Clinical Physiology and Functional Imaging* 29.5, pp. 353–359.

Ahlgren, Å. R., Steen, S., Segstedt, S., Erlöv, T., Lindström, K., Sjöberg, T., Persson, H. W., Ricci, S., Tortoli, P., and Cinthio, M. (2015). "Original Contribution: Profound Increase in Longitudinal Displacements of the Porcine Carotid Artery Wall Can Take Place Independently of Wall Shear Stress: A Continuation Report." In: *Ultrasound in Medicine & Biology* 41.5, pp. 1342–1353.

Albinsson, J., Brorsson, S., Ahlgren, Å. R., and Cinthio, M. (2014). "Improved tracking performance of Lagrangian block-matching methodologies using block expansion in the time domain: in silico, phantom and in vivo evaluations." In: *Ultrasound In Medicine & Biology* 40.10, pp. 2508–2520.

Cinthio, M., Jansson, T., Persson, H. W., Lindström, K., Eriksson, A., and Ahlgren, Å. R. (2005). "Evaluation of an ultrasonic echo-tracking method for measurements of arterial wall movements in two dimensions." In: *IEEE Transactions on Ultrasonics, Ferroelectrics, and Frequency Control* 52.8, pp. 1300–1311.

Cinthio, M., Ahlgren, Å. R., Bergkvist, J., Jansson, T., Persson, H. W., and Lindström, K. (2006). "Longitudinal movements and resulting shear strain of the arterial wall." In: *American Journal of Physiology: Heart & Circulatory Physiology* 60.1, pp. 394–402.

Encyclopedia Britannica (2015). *Agar*. URL: http://academic.eb.com/EBchecked/topic/8750/agar (visited on 04/01/2015).

Gijsen, F. J. H., Van De Vosse, F. N., and Janssen, J. D. (1999). "The influence of the non-Newtonian properties of blood on the flow in large arteries: Steady flow in a carotid bifurcation model." In: *Journal of Biomechanics* 32.6, pp. 601–608.

Hoskins, P., Martin, K., and Thrush, A. (2010). *Diagnostic ultrasound : physics and equipment.* Cambridge : Cambridge University Press.

Kwon H. M.and Kang, S., Hong, B. K., Kim, D., Park, H. Y., Shin, M. S., and Byun, K. H. (1999). "Ultrastructural Changes of the External Elastic Lamina in Experimental Hypercholesterolemic Porcine Coronary Arteries." In: *Yonsei Medical Journal* 40.3, pp. 273–282.

Laurent, S., Cockcroft, J., Van Bortel, L., Boutouyrie, P., Giannattasio, C., Hayoz, D., Pannier, B., Vlachopoulos, C., Wilkinson, I., and Struijker-Boudier, H. (2006). "Expert consensus document on arterial stiffness: methodological issues and clinical applications." In: *European Heart Journal* 27.21, pp. 2588–2605.

Laurent, S., Boutouyrie, P., Asmar, R., Gautier, I., Laloux, B., Guize, L., Ducimetiere, P., and Benetos, A. (2001). "Aortic Stiffness Is an Independent Predictor of All-Cause and Cardiovascular Mortality in Hypertensive Patients". In: *Hypertension* 37, pp. 1236–1241.

Lindgärde, F., Thulin, T., and Östergren, J. (2009). *Kärlsjukdom : vaskulär medicin.* Lund : Studentlitteratur.

Mendis, S., Puska, P., and Norrving, B., eds. (2011). *Global atlas on cardiovascular disease prevention and control Policies, strategies and interventions*. Geneva: World Health Organization.

Nationalencyklopedin (2015a). *Adrenalin*. URL: www.ne.se/uppslagsverk/encyklopedi/l%C3%A5ng/adrenalin (visited on 02/11/2015).

— (2015b). *Blodtryck*. URL: http://www.ne.se/uppslagsverk/encyklopedi/l%C3%83%C2%A5ng/blodtryck (visited on 04/13/2015).

Nichols, W. W. and O'Rourke, M. F. (2005). *McDonald's Blood Flow in Arteries: Theoretical, Experimental and Clinical Principles. Fifth edition*. London: Hodder Arnold.

Purwanto, Eswaran, C., Logeswaran, R., and Rahman, A. R. A. (2012). "Prediction Models for Early Risk Detection of Cardiovascular Event." In: *Journal of Medical Systems* 36.2, pp. 521–531.

Sigma-Aldrich (2015). *Poly(vinyl alcohol)*. URL: http://www.sigmaaldrich.com/catalog/product/aldrich/341584?lang=en%5C&region=SE (visited on 04/01/2015).

Young, D. F., Munson, B. R., and Okiishi, T. H. (2004). *A Brief Introduction to Fluid Mechanics, Third Edition*. Hoboken, NJ: John Wiley & Sons, INC.

Zahnd, G., Vray, D., Sérusclat, A., Alibay, D., Bartold, M., Brown, A., Durand, M., Jamieson, L., Kapellas, K., Maple-Brown, L. J., O'Dea, K., Moulin, P., Celermajer, D., and Skilton, M. R. (2012). "Longitudinal displacement of the carotid wall and cardiovascular risk factors: associations with aging, adiposity, blood pressure and periodontal disease independent of cross-sectional distensibility and intima-media thickness." In: *Ultrasound in Medicine & Biology* 38.10, pp. 1705–1715.

Zamir, M. (2000). *The Physics of Pulsatile Flow*. New York: Springer-Verlag New York INC.